Tunneling spectroscopy of the superconducting energy gap in $R\mathrm{Ni_2B_2C}$ (R=Y and Lu)

Toshikazu Ekino* and Hironobu Fujii
Faculty of Integrated Arts and Sciences, Hiroshima University, Higashi-Hiroshima 739, Japan

Makoto Kosugi, Yuji Zenitani, and Jun Akimitsu
Department of Physics, Aoyama-Gakuin University, Setagaya, Tokyo 157, Japan
(Received 6 October 1995)

Superconducting energy gap in $R\mathrm{Ni_2B_2C}$ (R=Y and Lu) has been investigated using a break-junction tunneling technique. The observed differential conductance dI/dV is well described by the BCS density of states with a small lifetime broadening parameter. We have found small gap values for the local low-T_c phases in addition to the bulk T_c of 15.6–16.6 K. The gap value of 2Δ=4.5 meV with T_c=15 K gives the BCS ratio of $2\Delta/k_BT_c$=3.5, which is kept constant down to the observed lowest T_c of 4.6 K. These results give clear evidence for the BCS mechanism of superconductivity for these compounds.

INTRODUCTION

The appearance of superconducting quaternary intermetallic borocarbides $RT_2\mathrm{B_2C}$ (R=rare earth, T=transition metal) has offered an opportunity to explore the research field of intermetallic high-temperature superconductors, in addition to the copper and noncopper oxides, and metal-doped fullerene solids.[1,2] $R\mathrm{Ni_2B_2C}$ contains a $3d$-transition-metal Ni, which would imply strong electron correlations, light-mass elements B and C, and $\mathrm{Ni_2B_2}$ layers stacking alternately with RC planes.[3] These characteristics somewhat resemble those of the copper oxide superconductors. Therefore it is interesting to have insight into the superconductivity mechanism of this compound. The superconducting transition temperature T_c of $R\mathrm{Ni_2B_2C}$ varies from 7.5 K (R=Ho) to the highest value of 16.6 K (R=Lu) among the Ni borocarbide intermetallics.[2] More significantly, a high T_c of $\approx$22–23 K has been found in both $\mathrm{YPd_2B_2C}$ (Ref. 4) and Th-Pd-B-C (Ref. 5), the value of which is higher than any other intermetallic compounds. The T_c's of these compounds are comparable to those for the other well-known strong-coupling high-T_c intermetallic $A15$ superconductors.[6] The $R\mathrm{Ni_2B_2C}$ compound possesses the electronic specific-heat coefficient γ of 20–35 mJ/mol K^2,[7] which is the same magnitude as those for the $A15$ compounds. The upper critical field $H_{c2}\approx$10 T for $R\mathrm{Ni_2B_2C}$ is much lower than 20–40 T for the $A15$ compounds.[8] The origin of the relatively large γ values of $R\mathrm{Ni_2B_2C}$ favorable to a high T_c is mainly due to the narrow and large Ni $3d$ electronic states near E_F.[9,10] The values of the coherence length $\xi\gtrsim$5 nm and the mean free path $l\approx$70 nm indicate a clean-limit superconductivity.[8] While the superconductivity in $R\mathrm{Ni_2B_2C}$ has been suggested to be strong coupling,[7,9] preliminary results of tunneling and Andreev reflection measurements showed weak-coupling BCS characteristics.[11–13] Furthermore, both a band-structure calculation[10] and an isotope experiment[14] showed that the high-energy optical phonons involving B atoms play an important role for the occurrence of superconductivity. Especially, the band-structure calculation pointed out a secondary role of Ni $3d$ electrons as strongly correlated states, thus suggesting a conventional superconductivity of these compounds.

In this paper we explore the energy gap of $R\mathrm{Ni_2B_2C}$ (R=Y,Lu) using tunneling spectroscopy to clarify the nature of this class of superconductivity. The tunneling technique is indispensable to observe the quasiparticle energy gap directly,[15] thereby enabling us to make a straightforward comparison with that of the other intermetallics such as $A15$ (Ref. 6) and the Chevrel compounds,[16] as well as copper and noncopper oxide superconductors.[17]

EXPERIMENTAL DETAILS

The crystal structure of $R\mathrm{Ni_2B_2C}$ is a filled version of the tetragonal-body-centered $\mathrm{ThCr_2Si_2}$ type (an ordered variant of the $\mathrm{BaAl_4}$ type).[2] The compounds with this structure have played an important role for exploring the heavy Fermion physics.[18] Polycrystalline samples were prepared by arc melting under Ar gas and annealed in a vacuum-sealed quartz tube at 1100 °C for 35 h. The susceptibility measurements using a superconducting quantum interference device (SQUID) magnetmeter indicate that the sample of $\mathrm{YNi_2B_2C}$ cooled in zero field showed perfect diamagnetism, while on cooling it in a field of 10 Oe a Meissner volume fraction of 27% was obtained. For $\mathrm{LuNi_2B_2C}$, 22% of perfect diamagnetism was obtained for zero-field cooling. The onset T_c was 15.6 and 16.6 K for R=Y and Lu, respectively. The widths of T_c obtained from the volume fraction of 10–90% to the saturated diamagnetism were approximately 2.3 K (R=Y) and 0.7 K (R=Lu). The latter exhibits a much sharper transition than the former in spite of the smaller volume fraction. Tunneling measurements were carried out using break junctions that are believed to provide a fresh and unaffected interface.[12,19] A polycrystalline sample having a cross section of approximately 1.5×0.5 mm^2 was mounted on a flexible substrate to crack under liquid-helium temperature by applying adjustable bending force, and then the cracked sample pieces were brought together by releasing the bending force until the tunneling current was able to be detected. The differential conductance dI/dV of the current (I)-voltage (V) characteristics was directly obtained by an ac modulation technique using a four-probe method.

RESULTS AND DISCUSSION

For the break-junction geometry, a superconductor-insulator-superconductor (SIS) tunneling is expected for cracking the sample at intragrains. In this case, the gap value of 4Δ would be obtained. However, a gap of 2Δ from the superconductor-insulator-normal (SIN) tunneling was also often observed in our measurements. This is probably because the sample is cracked at grain boundaries and one side of the interface region is in the normal state. For the polycrystalline samples, the grain boundaries may be brittle and chemically complex because their compositions are different from the main phase of $R\mathrm{Ni_2B_2C}$. This would explain why the cracking often occurs at grain boundaries. Furthermore, we have obtained several small gap values corresponding to low-T_c phases in numbers of the tunnel junctions, which is probably due to local variations in compositions. It should be noted, however, that the x-ray- diffraction data showed a single phase and no secondary phase was evident in the SQUID data for the samples used in the present measurements. Therefore we speculate that such low-T_c phases are mainly located along the grain boundaries that are extended in the whole sample, but are a very small amount. The distributed gap feature observed here allowed us to investigate the T_c dependence of the gap value. The local T_c distributions were also manifested in the NMR and specific-heat measurements which could probe the low-energy quasiparticle excitations.[7,20] Notice that these features somewhat resemble the case of $\mathrm{ThCr_2Si_2}$-type polycrystalline compounds, where a microprobe analysis clarified the existence of a secondary phase at the grain boundaries, even if the x-ray-diffraction data showed a single phase.[21] Such a small stoichiometric variation often would cause a drastic change in the electronic properties.[22]

For interpreting the observed spectra, density-of-states fitting procedures should be performed to distinguish between the SIS and SIN tunnelings. Among several fitting functions,[17] the lifetime-broadened BCS densities of states[23] with thermal smearing were found to fit well to the most of the experimental data with a small broadening parameter for the SIS junction and slightly larger value for the SIN case. We consider that the above difference is most likely due to the difference in the surface quality, which is higher for intragrain cracking of the SIS tunneling than that for intergrain one of the SIN case.

Figure 1(a) shows the tunneling conductance dI/dV for a $\mathrm{LuNi_2B_2C}$ break junction. The conductance curve quite resembles that of the SIS junction of the standard BCS superconductor with no Josephson supercurrent. The junction resistance of $R_J=54$ kΩ at the gap edge of 4.5 mV and the critical current density $J_c\approx10^5$–10^6 A/cm^2 (Ref. 24) give the possible smallest effective junction area that retains superconductivity to be $\approx10^{-10}$–10^{-11} mm^2. This is significantly smaller than the nominal junction area of ≈1 mm^2. However, from the sharpness of the gap-edge peaks and absence of the Josephson current, the high R_J value here can be due to a thicker insulating barrier where the actual current density should be low enough. Therefore the junction area would be much larger than the estimated value.

We compare the experimental data with the calculated tunneling density of states for the SIS junction,[15]

$$dI(V)/dV=d\left[C\int_{-\infty}^{+\infty}N(E,\Gamma)N(E+eV,\Gamma)[f(E)-f(E+eV)]dE\right]/dV, \tag{1}$$

using a lifetime-broadened BCS density of states proposed by Dynes *et al.*[23]

$$N(E,\Gamma)=\mathrm{Re}\{(E-i\Gamma)/[(E-i\Gamma)^2-\Delta^2]^{1/2}\}, \tag{2}$$

where Γ, C, $f(E)$, and Δ are a phenomenological broadening parameter, the scaling parameter, the Fermi distribution function, and the energy gap, respectively. The values of Δ, Γ, and C were chosen to fit the peak position and height and the background conductance of the experimental data. Consequently, the calculated curve explains well the experimental data, especially the sharp rise at the gap edge as shown in Fig. 1(b) for $T=4.2$ K, $\Delta=2.23$ meV, and $\Gamma=0.17$ meV. The sharp gap structure of $V_{\mathrm{p.-p.}}=9$ mV is therefore attributed to $4\Delta_{\mathrm{p.-p.}}/e$ of the SIS junction, where $\Delta_{\mathrm{p.-p.}}$ is defined by the peak-to-peak separation of dI/dV for the SIS junction divided by 4. The subgap structures at $\pm\Delta_{\mathrm{p.-p.}}/e\approx\pm2.2$–$2.3$ mV for the calculated curve are not observed in the experimental data. The observed conductance exhibit a broadened weak zero-bias hump, but it is almost flat in the region well above the gap voltage. The pronounced conductance dips just above the gap voltages can be due to a surface proximity effect.[25] Such structures are produced by both the rapid conductance decrease just above the gap voltage caused by the Andreev reflection and the increase of the quasiparticle conductance above it. We have not measured the temperature variations of this spectrum, but the ratio $2\Delta_{\mathrm{p.-p.}}/k_BT_c=3.4$ obtained by $4\Delta_{\mathrm{p.-p.}}=8.9$ meV and $T_c=15.2$ K (90% of the full transition) from the SQUID data indicates a weak-coupling superconductivity. Note that we have not often observed the above gap values, thereby demonstrating that the cracked junction interface usually differs from the bulk T_c phase.

Figure 2 presents the tunneling conductance from another SIS junction. The $R_J\approx5.7$ kΩ well above the gap is $\approx1/40$ of that in Fig. 1. The intensive peaks at $\pm2\Delta_{\mathrm{p.-p.}}/e$ and the proximity-effect-induced dips above the gap voltages are similar to those in Fig. 1. The smaller value of $2\Delta_{\mathrm{p.-p.}}/e=3.8$ mV of Fig. 2 than 4.5 mV of Fig. 1 may be due to local T_c variation of the sample. Also visible in Fig. 2 is the peak structures at $\pm(2\Delta_{\mathrm{p.-p.}}/e)/2=\pm1.9$ mV, the broad humps around $\pm(2\Delta_{\mathrm{p.-p.}}/e)/3=\pm1.2$–$1.3$ mV, and the zero-bias peak. These features may be a consequence of a relatively

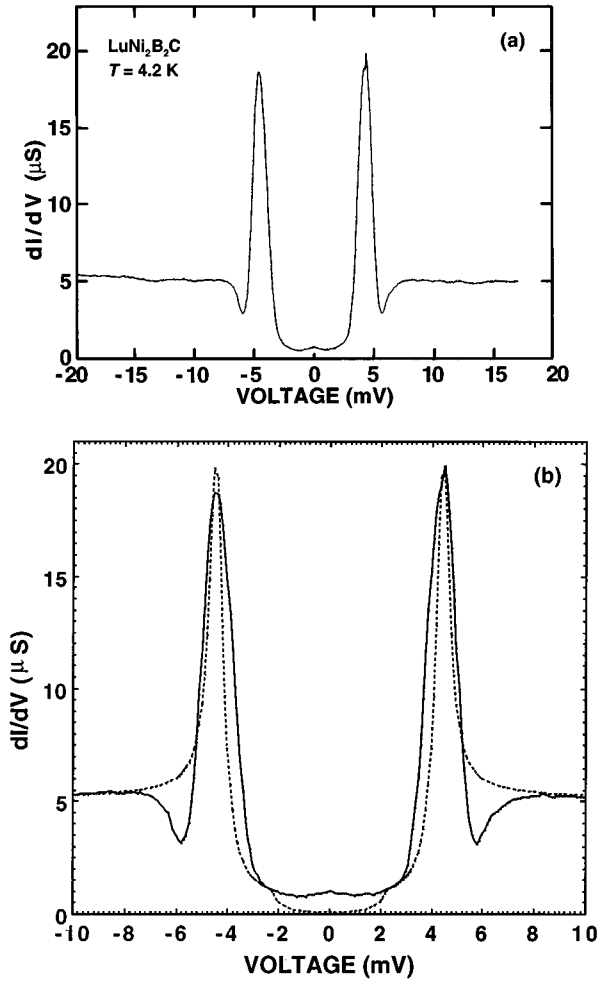

FIG. 1. (a) Tunneling conductance for a $LuNi_2B_2C$ polycrystal break junction at 4.2 K. (b) Comparison of the experimental data (dashed line) with the calculated tunneling conductance for a SIS junction using Eqs. (1) and (2) with $T=4.2$ K, $\Delta=2.23$ meV, and $\Gamma=0.17$ meV (solid line).

high barrier transparency at the junction interface. The subgap structures of $(2\Delta_{p.\text{-}p.}/e)/n$ $(n=2,3)$ observed in Fig. 2 give evidence for the multiparticle (n-particle) tunneling and/or the multiple Andreev reflection processes for the SIS junction, which are absent in the SIN junction.[26–28]

As mentioned above, we have often observed the smaller $\Delta_{p.\text{-}p.}$ values. The observed smallest sharp-gap structures are shown in Figs. 3 and 4 for $LuNi_2B_2C$, together with the I-V characteristics. These structures are due to the SIS gap because they are much sharper than the ideal BCS singularity expected for the SIN tunneling. In Fig. 3, the gap-edge peaks occur at $\pm 2\Delta_{p.\text{-}p.}/e=\pm 2.8$ mV and the weak humps at ± 1.4 mV correspond to $\pm\Delta_{p.\text{-}p.}/e$. On the other hand, the tunneling conductance of Fig. 4 possesses $4\Delta_{p.\text{-}p.}=3.2$ meV with the smooth conductance feature inside the gap voltage. In particular, a flat region observed around zero bias cannot be reproduced by the calculation using Eqs. (1) and (2) even if we put $\Gamma=0$ meV. In Figs. 3 and 4, there are no conductance dips owing to a proximity effect unlike the cases of Figs. 1 and 2. Such dips were also not observed for the smaller-gap structures in the present measurements as shown in Figs. 5, 9, 13, and 14, presumably reflecting the difference in the

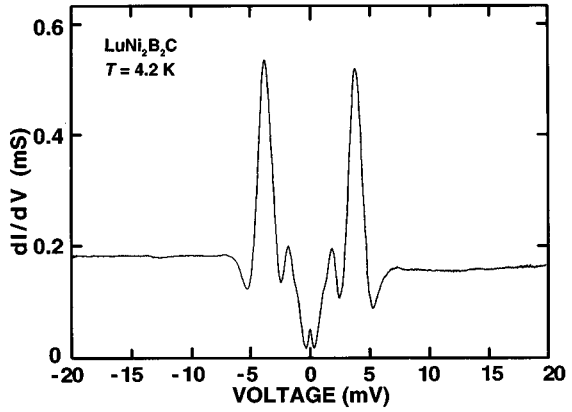

FIG. 2. Tunneling conductance for a $LuNi_2B_2C$ break junction at 4.2 K.

characteristics of the interface regions of the junction between the bulk and other phases.

It is noted that in the sharp-gap structure the phonon excitations would be observable above the gap energy for the strong-coupling superconductors.[6,15] In fact, using the break junction, we have observed clear phonon structures in Pb at the correct energies. However, in Figs. 3 and 4 such structures are not observed within a resolution of an at least >0.1–0.5% change of the conductance above the gap voltage. This is consistent with the weak-coupling nature where the phonon structures would be hardly observed. This situation is similar to the case of $Ba_{0.6}K_{0.4}BiO_3$ $(2\Delta/k_BT_c=3.5)$,

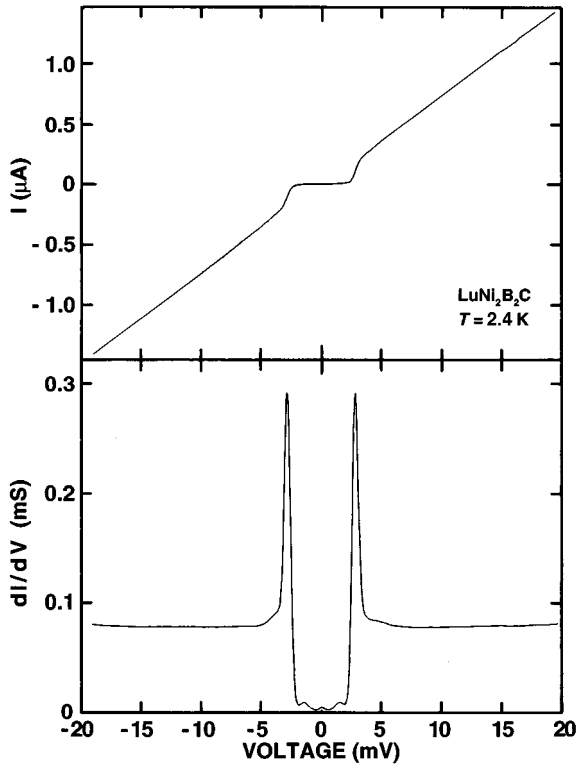

FIG. 3. I-V characteristics (top) and dI/dV (bottom) for a $LuNi_2B_2C$ break junction with $4\Delta_{p.\text{-}p.}=5.6$ meV at 2.4 K.

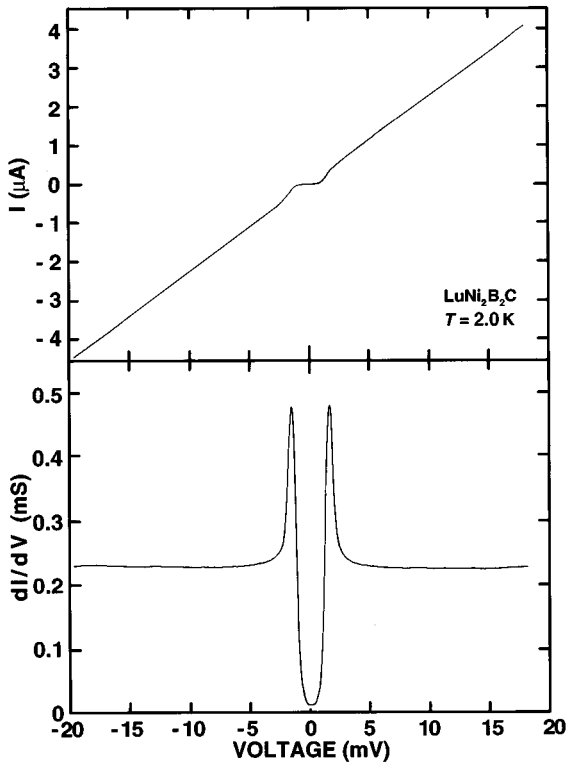

FIG. 4. I-V characteristics (top) and dI/dV (bottom) for a $LuNi_2B_2C$ break junction with $4\Delta_{p.-p.}=3.2$ meV at 2.0 K.

in which the phonon structures were observed only very weakly.[29] the measurement beyond ± 20 mV would be desirable to clarify the contribution of high-energy phonons as was suggested by an isotope-effect measurement and the band-structure calculation.[10,14]

Figure 5(a) shows the tunneling conductance from an YNi_2B_2C SIS junction, where the large zero-bias peak as well as the peaks at ± 2.2 mV are evident. As shown in Fig. 5(b), the observed tunneling conductance, except the zero-bias peak, is well described by the SIS model using Eqs. (1) and (2) for $T=4.2$ K, $\Delta=1.10$ meV, and $\Gamma=0.11$ meV. The zero-bias features are largely different from each other, but the intensive peak in the experimental curve is partly reproduced by the calculation. This is due to a finite tunneling probability of the quasiparticles between the subgap states of opposing electrodes, which are induced by Γ and T even at thermal equilibrium (i.e., $V=0$). The remaining component of the observed zero-bias peak probably comes from a Josephson or weak-link supercurrent. Notice that the broadened feature in Fig. 5 ($\Gamma/\Delta=0.1$) is similar to that for Fig. 1 (≈ 0.08).

In Fig. 6, the high-bias feature of the tunneling conductance of Fig. 3 is presented with the bias voltages extended up to ± 320 mV. The background conductance above $\pm\Delta/e$ is symmetric with respect to zero bias, having the total change of it about 70–80% at ± 320 mV. Assuming that the heating effect of the junction is negligible because of the relatively high R_J of 3–6 kΩ and the smoothly increasing conductance with increasing bias voltage, we have fitted the simple tunneling model with a rectangular barrier at 0 K to the conductance of Fig. 6,[15]

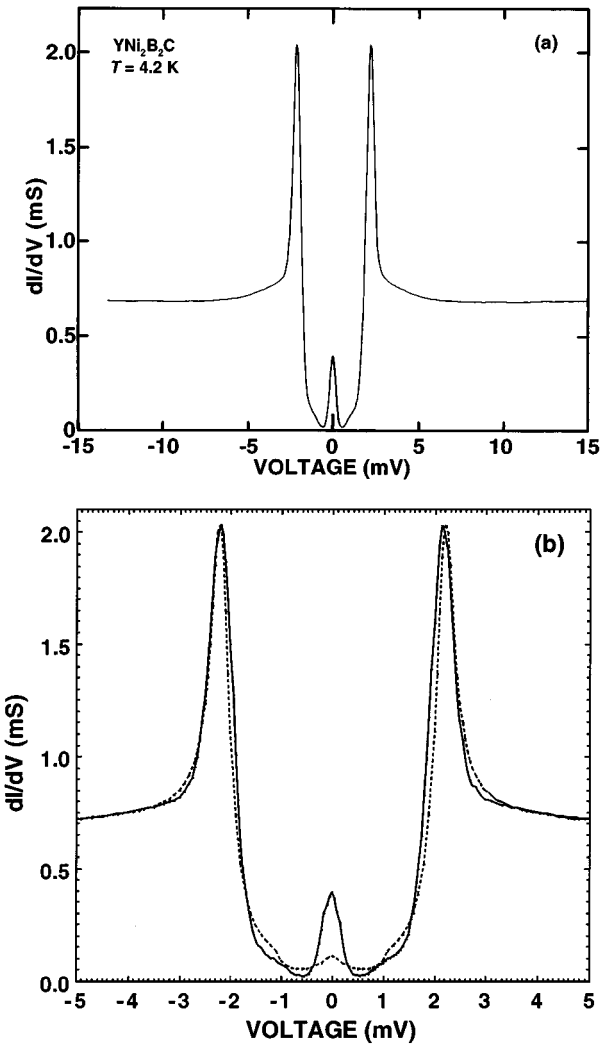

FIG. 5. (a) Tunneling conductance for an YNi_2B_2C break junction at 4.2 K. (b) Comparison of the conductance (dashed line) with the calculation using Eqs. (1) and (2) for $T=4.2$ K, $\Delta=1.10$ meV, and $\Gamma=0.11$ meV (solid line).

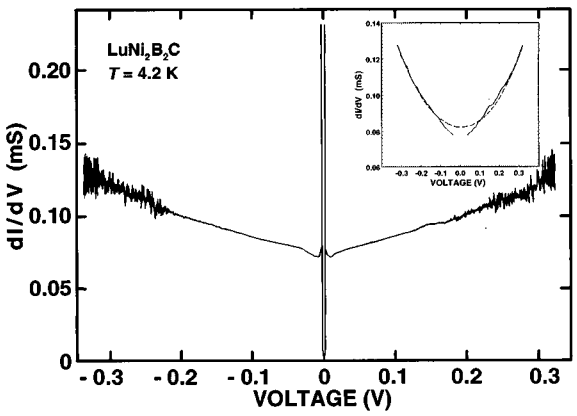

FIG. 6. High-bias tunneling conductance for the same $LuNi_2B_2C$ junction as that in Fig. 3. Inset: comparison of the experimental data (solid line) with the calculated tunneling conductance using Eq. (3) (dashed line).

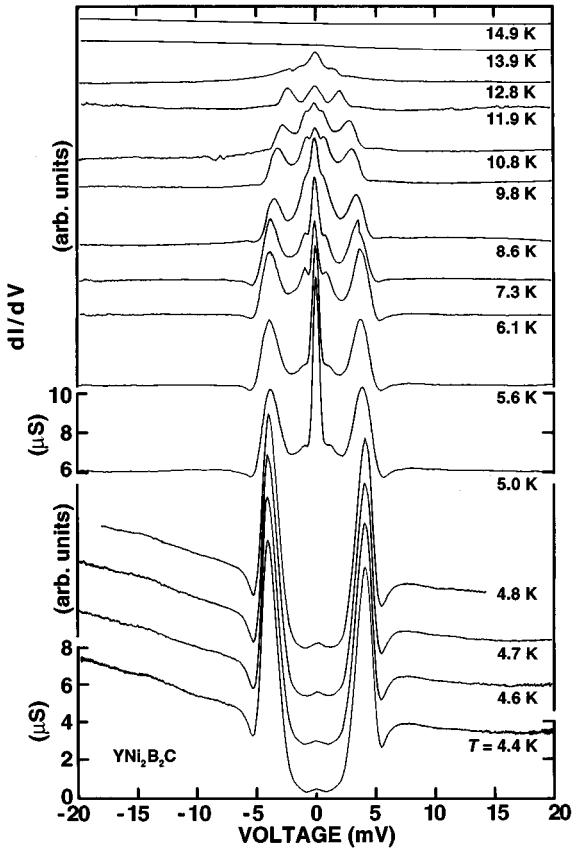

FIG. 7. Temperature variations in tunneling conductance from an YNi_2B_2C break junction with $4\Delta_{p.-p.}=8.1$ meV at 4.2 K.

$$dI(V)/dV = C(U_B - eV/2)^{1/2} t^{-1} \cosh[(m/2)^{1/2}\hbar^{-1} etV(U_B - eV/2)^{-1/2}], \quad (3)$$

where U_B and t are the barrier height and thickness, respectively. Equation (3) tells us that the thicker (thinner) barrier results in the stronger (weaker) bias dependence for the constant U_B. The experimental data do not exhibit a simple parabolic shape expected from Eq. (3) for $eV \ll U_B$, but we were able to choose the appropriate values of $U_B=5$ eV and $t=0.7$ nm to explain the bias dependence of the background conductance, as shown in the inset of Fig. 6. The relatively large value of U_B for a mechanically stable junction as in this case suggests the formation of an insulating material barrier rather than the vacuum barrier.

For evaluating the ratio $2\Delta/k_B T_c$ from the distributed gap values presented in Figs. 1–5, it is necessary to obtain T_c by measuring the temperature dependence of the tunneling conductance itself. Although the break junction had been considered to be unstable against temperature change, we were able to obtain the available data. An example of the temperature variations of dI/dV from an YNi_2B_2C SIS junction is displayed in Fig. 7 with $4\Delta_{p.-p.}=8.1$ meV at 4.2 K. The asymmetric background conductance is evident at low temperatures, and the R_J at high-bias voltages are almost of the same magnitude as that in Fig. 1. With increasing temperature the R_J slightly changes at about 5 K, thereby resulting in the drastic change of the conductance curve where the flat background conductance and the large zero-bias peak appear

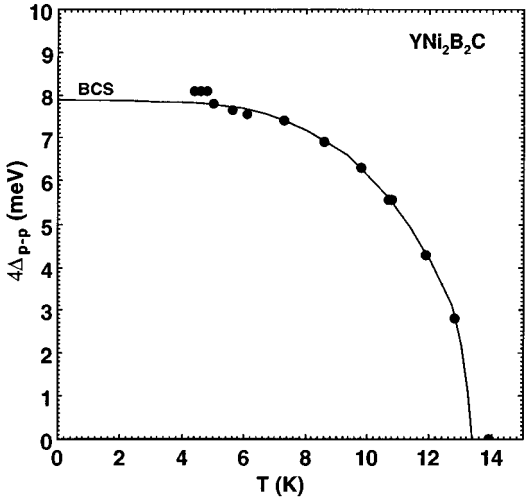

FIG. 8. Temperature dependence of the energy gap $4\Delta_{p.-p.}$ from Fig. 7.

with shoulderlike peaks at ± 1 mV. The origin of the zero-bias peak is probably due to the Josephson supercurrent and/or leak current through a weak link.[27] The subgap peaks at ± 1 mV above 5 K can be due to $\pm(\Delta_{p.-p.}/e)/2$ of the multiple Andreev reflections between two superconductors, which are expected to be intensive for the weak-link junction.[28] As shown in Fig. 7, the intensities of both the zero-bias peak and the peaks of $\pm 2\Delta_{p.-p.}/e = \pm 3.8 - 3.9$ mV at 5 K smoothly decrease with increasing temperature. In par-

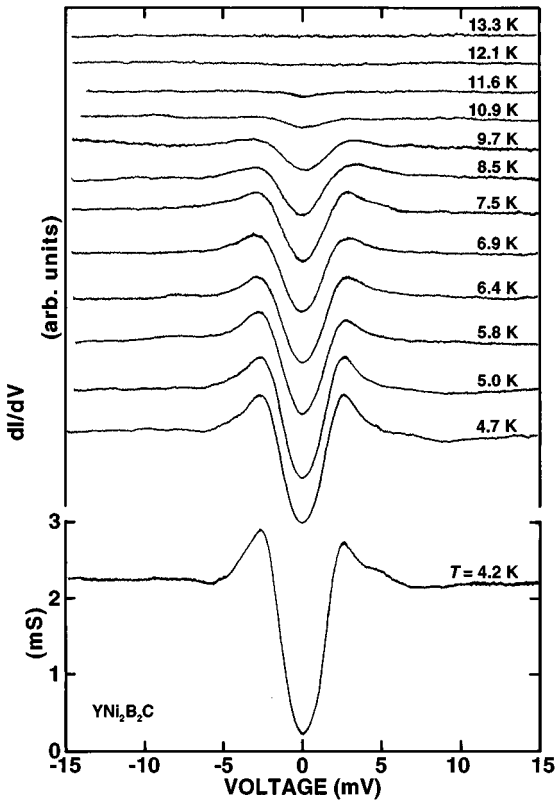

FIG. 9. Temperature variations in tunneling conductance from an YNi_2B_2C break junction.

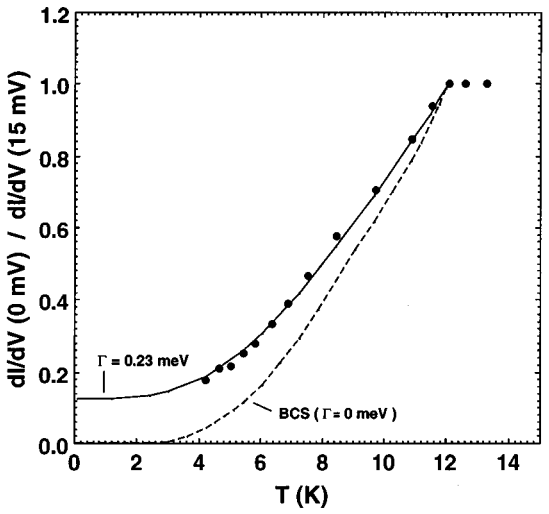

FIG. 10. Temperature dependence of the normalized zero-bias conductance $dI/dV(0\ \mathrm{mV})/dI/dV(15\ \mathrm{mV})$ from Fig. 9. T_c is obtained as 12.1 K. Dashed and solid lines represent the calculations using $N(E,\Gamma)$ [Eq. (2)] with $\Gamma=0$ (BCS) and 0.23 meV, respectively.

ticular, the gap peak positions shifting to low energies are clearly observed because of the crossing of density-of-states singularities between the opposing electrodes. They are well defined up to T_c, as is expected for the ideal SIS tunneling.[15]

Figure 8 shows the temperature dependence of $4\Delta_{\mathrm{p.-p.}}$ obtained from Fig. 7. The data points perfectly agree with the BCS prediction over the whole temperature range except for low temperatures where the junction condition is slightly different. Thus the extrapolated values of $4\Delta_{\mathrm{p.-p.}}=7.9-8.1$ meV at 0 K and $T_c=13.4$ K from this curve give the ratio $2\Delta_{\mathrm{p.-p.}}/k_BT_c=3.4-3.5$, being in agreement with the BCS value.

Figure 9 shows the temperature dependence of dI/dV for another YNi_2B_2C break junction. The conductance curve at 4.2 K is much broader than those of Figs. 1–6, but the leakage conductance at zero bias is considerably low. The junction with such a broadened characteristic was usually stable against the temperature variations. With increasing temperature the gap structure is thermally broadened and it merges with the background conductance without a shift of the peak energy, which is in contrast to Fig. 7, but in agreement with the standard BCS temperature dependence of the SIN tunneling conductance.

In Fig. 10, the temperature dependence of the normalized zero-bias conductance $dI/dV(0\ \mathrm{mV})/dI/dV(15\ \mathrm{mV})$ obtained from Fig. 9 is shown, which is proportional to the thermal smeared density of states at E_F. The $T_c=12.1$ K was obtained from the onset of the decrease owing to the gap opening. Since the $V_{\mathrm{p.-p.}}=5.4$ mV at 4.7 K in Fig. 9 seems to be too small for the SIS gap value for this T_c, we compare the experimental data with the calculated dI/dV for the SIN junction using[15]

$$dI(V)/dV=C\int_{-\infty}^{+\infty}N(E,\Gamma)[-df(E+eV)/dV]dE \quad (4)$$

and obtained Δ, Γ, and the scaling parameter C at each temperature.

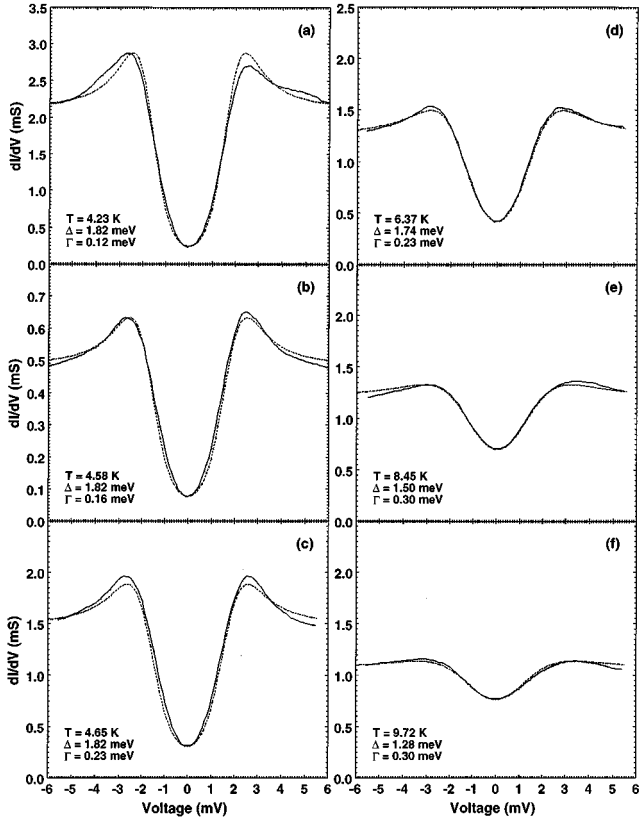

FIG. 11. Conductances of Fig. 9 fit with Eqs. (2) and (4) at several temperatures [(c)–(f)]. The data (a) and (b) are taken from the different junctions. Solid and dashed lines represent the experimental data and the calculated curve, respectively.

Figure 11 shows the fitting results at representative temperatures together with the data from different junctions possessing the similar $V_{\mathrm{p.-p.}}$ values at 4.2–4.6 K [Figs. 11(a) and 11(b)]. Remarkably, the experimental data are well fitted by Eq. (4), thereby indicating that only a life time broadening for the SIN tunneling accounts for the observed conductance feature. As is shown in Figs. 11(a)–11(c), the values of Δ [$\approx\Delta(0\ \mathrm{K})$ in this temperature range] are reproducible despite the significant differences in Γ [=(a) 0.12 meV, (b) 0.16 meV, and (c) 0.23 meV]. As is evident from the figure, all these Γ values explain well the leakage conductances for each curve. The values of $\Delta=1.82$ meV and $\Gamma=0.12-0.23$ meV at 4.2–4.7 K give the ratios of $2\Delta/k_BT_c=3.5$ and $\Gamma/\Delta=0.07-0.13$.

To clarify the difference in the conductance features between the SIN and SIS tunnelings for nonzero Γ values, we have calculated the conductances for both the junction geometries at 1.5 K using the experimental values of $\Delta=1.82$ meV and $\Gamma=0.23$ meV at 4.7 K and compared with each other. The results showed that for the SIN tunneling the value of $2\Delta_{\mathrm{p.-p.}}=4.23$ meV of the calculated conductance is a factor of 1.2 larger than the observed gap value of $2\Delta=3.64$ meV, while for the SIS case the calculated value of $4\Delta_{\mathrm{p.-p.}}=7.30$ meV agrees with the experimental value of $4\Delta=7.28$ meV. Therefore the fitting procedure is necessary to obtain Δ for the SIN tunneling, whereas the $\Delta_{\mathrm{p.-p.}}$ value gives a correct gap value for the SIS case. Since an unaffected junction interface is expected for the break junction, the nonzero Γ

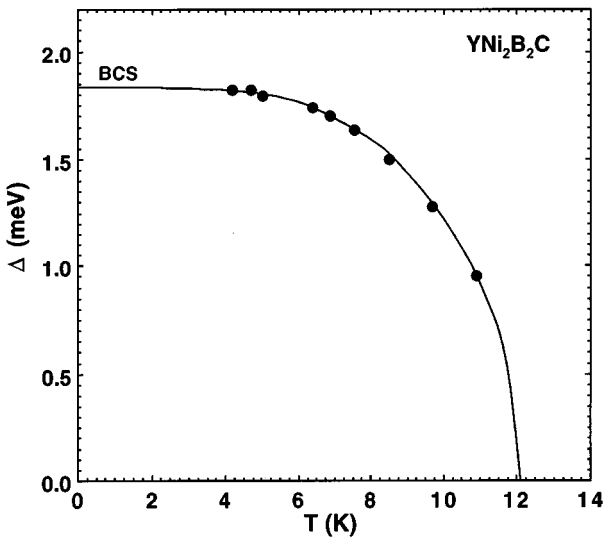

FIG. 12. Temperature dependence of Δ obtained from the fitting procedures as shown in Fig. 11 (solid circles). The solid line represents the BCS prediction.

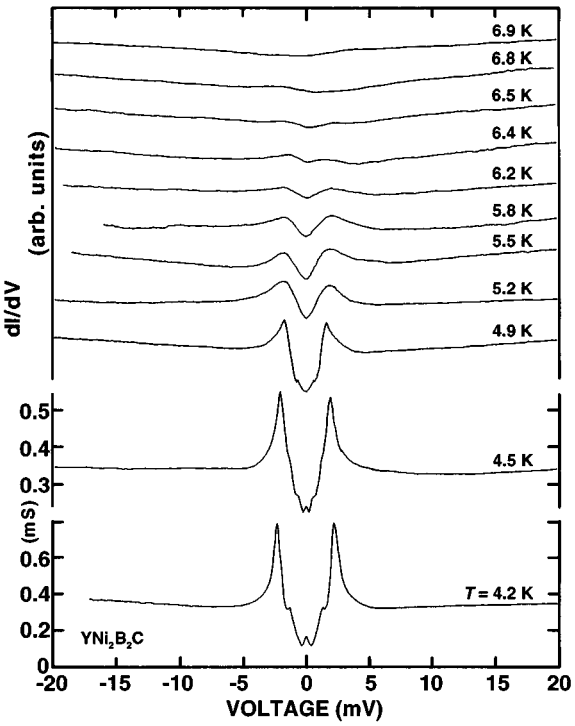

FIG. 13. Temperature variations in tunneling conductance from an YNi_2B_2C break junction with $4\Delta_{p.-p.}=4$ meV at 4.2 K.

value may not be a surface artifact. It may be related to the polycrystal grains and/or inhomogeniety, where the electrons have possibilities to go out or in between the superconducting and normal states through the grain boundaries. This would result in a finite lifetime of the quasiparticles in the superconducting state. The larger Γ values for the SIN tunneling than that for the SIS case as shown in Figs. 1, 5, and 11 can be explained by the much degradated junction-interface characteristics consisting of grain boundaries for the SIN junction compared to the cracked junction interface for the SIS junction.

The fitting results like in Fig. 11 demonstrate that the anisotropic gap is not the case for the RNi_2B_2C compound, because all the gap features are well described by only the Γ term and the probability-distribution function of the gaps is not needed.[17] The above results are therefore consistent with the nearly isotropic electronic properties of RNi_2B_2C.[30] This feature is in contrast with, for example, the cuprate superconductivity with CuO_2 layers, where the Gaussian gap-distribution model often describes the observed gap broadening.[17]

In Fig. 12, the values of Δ from the above fitting procedures are plotted as a function of temperature, where the BCS temperature dependence of Δ is clearly visible. It is noted that Γ is almost constant or slightly increases with increasing temperature, probably reflecting the fact that the interface characteristics do not depend on temperature. Since Γ is the only parameter which describes the zero-bias conductance for the given Δ and T, we have calculated the temperature dependence of dI/dV(0 mV) with Γ. The best fit to the experimental data in a whole temperature range is obtained for $\Gamma=0.23$ meV ($=2.7$ K) as shown by the solid line in Fig. 10. From Figs. 8 and 12, it is obvious that the sharp gap-peak positions for the SIS tunneling (Fig. 8) and the conductance-fitted gap values for the SIN tunneling (Fig. 12) actually match with the BCS temperature dependence. This feature is in contrast to the results of specific-heat and nuclear spin-lattice relaxation measurements, which suggest a deviation from the simple BCS picture.[7,20]

In the present work, we have probed much smaller gap values than that corresponding to the bulk T_c of RNi_2B_2C. Figure 13 shows such data for YNi_2B_2C with the temperature variations of dI/dV having $eV_{p.-p.}=4$ meV at 4.2 K and $R_J\approx 2.5$ kΩ at high bias. These values are similar to those in Fig. 5. The significant features of Fig. 13, namely, the sharper gap peaks than those for the SIN tunneling at 4.2 K and the existences of the inner gap at ±1 meV and the zero-bias peak, give evidence for the SIS junction with $4\Delta_{p.-p.}=4$ meV. With increasing temperature the gap structure gradually smears out, displaying no apparent shift of its peak position. This is because the gap closing and temperature broadening balance each other on warming up as in the case of SIN tunneling, the feature being in contrast to the temperature shift of $\Delta_{p.-p.}$ for the standard SIS tunneling as is seen in Fig. 7. The T_c of 6.7 K obtained from the temperature where the gap structure disappears as shown in Fig. 13 is very low compared to the bulk T_c, but in agreement with that of $ThNi_2B_2C$, which has a bulk T_c of 6.3 K, close to the lower boundary reported in the literature.[31] This clearly demonstrates that we have observed the local properties with the composition being different from the stoichiometric RNi_2B_2C phase. Since the lowest temperature of 4.2 K in Fig 13 corresponds to T/T_c $(=t)=0.63$, thermal smearing is rather significant. Moreover, the gap feature is much broadened compared to the ideal SIS tunneling, in which $V_{p.-p.}$ no longer gives the correct gap value. From the numbers of our tunneling data showing the broadened gaps, the relationship of $\Delta=(0.8-0.9)\Delta_{p.-p.}$ for $t<0.5-0.6$ was empirically obtained.[17] By combining this with the ratio Δ $(t=0)/\Delta$ $(t=0.63)=1.1$ from BCS theory,[15] the relationship of

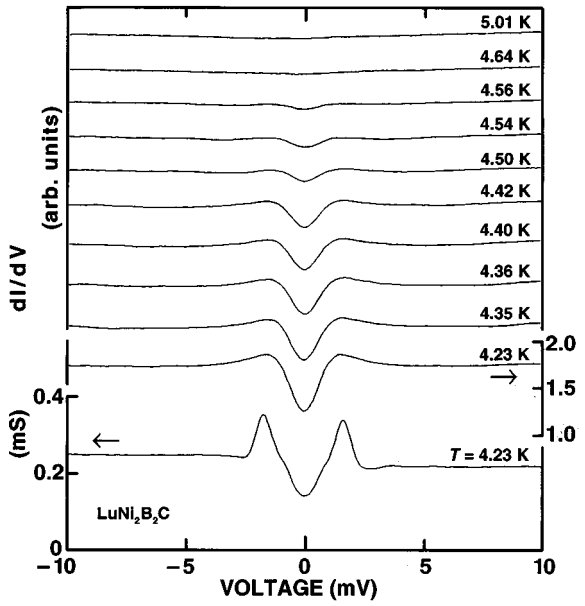

FIG. 14. Tunneling conductance of a $LuNi_2B_2C$ break junction at various temperatures. Junction conditions for the bottom curve are different from that of the other data in this figure.

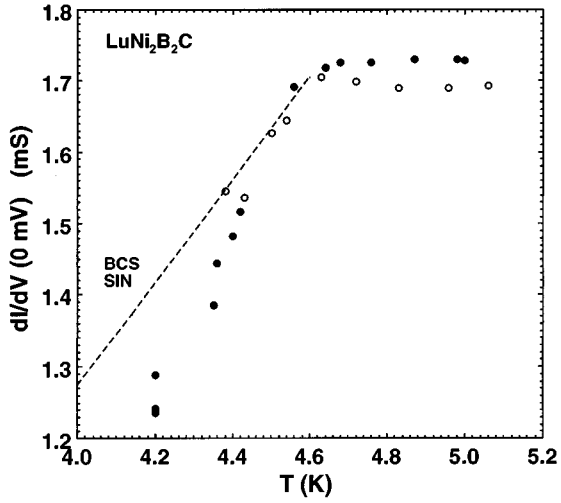

FIG. 15. Temperature dependence of $dI/dV(0\ \mathrm{meV})$ from Fig. 14. $T_c=4.6$ K. Solid and open circles correspond to heating and cooling processes, respectively. The dashed curve represents the BCS prediction for the SIN junction.

$\Delta\ (t=0)\approx\Delta_{\mathrm{p.-p.}}\ (t=0.63)$ is obtained. Therefore 2Δ would become ≈ 4 meV at 0 K, thereby giving the ratio $2\Delta/k_BT_c=3.5$.

Further, we have found a considerably low T_c of 4.6 K for a $LuNi_2B_2C$ junction. While the Ni-site substitution on $YNi_{2-x}T_xB_2C$ [T=Co (x=0.1), Fe (x=0.07), Ru] showed a decrease in T_c down to about 6 K,[32] the RNi_2B_2C compound with the bulk $T_c<5$ K has not yet been reported. In the present work, we use the lowest-T_c phase to probe the smallest gap size just before causing the superconducting phase to disappear in this compound. Figure 14 shows the temperature variations of dI/dV having the $eV_{\mathrm{p.-p.}}=3.2$ meV at 4.2 K. This value roughly agrees with that in Fig. 4, but the measuring temperature is different. In Fig. 14, mechanical instability of the junction did not allow us to measure the spectra below 4.2 K. The gap structure is rapidly smeared out on warming up to 5 K, but it is fairly well pronounced even at 4.2 K. The $T_c=4.6$ K is obtained from the temperature dependence of the zero-bias conductance $dI/dV(0\ \mathrm{mV})$ as shown in Fig. 15, where the onset of the gap opening is clearly seen. The temperature dependence of the $dI/dV(0\ \mathrm{mV})$ for the SIN junction calculated using the ideal BCS density of states is also presented in the figure. Since the experimental data are always below the ideal characteristics for the SIN tunneling given by the calculation, they are apparently due to the SIS tunneling. The tunneling conductance with the different R_J as shown in the bottom of Fig. 14 gives further evidence for the SIS gap. It displays the broad humps around $\pm V_{\mathrm{p.-p.}}/4=\pm\Delta_{\mathrm{p.-p.}}/e$, in addition to $\pm 2\Delta_{\mathrm{p.-p.}}/e$. Because of the SIS tunneling, the gap structure is well defined even at 4.2 K ($t=0.91$). For temperatures up to 4.56 K ($t=0.99$), the broadened gap feature at $\pm 2\Delta_{\mathrm{p.-p.}}/e=\pm 1.6$ mV shows no temperature shift, being similar to the case of Fig. 13. Although the gap feature is simply broadened with the constant background conductance, the fitting results using Eq. (1) were not satisfactory. Therefore, by considering the temperature broadening of the gap edge that results in a constant $V_{\mathrm{p.-p.}}$ on warming as discussed in Fig. 13, the gap value of $2\Delta=1.2$–1.4 meV at 0 K would be obtained from the $2\Delta_{\mathrm{p.-p.}}=1.6$ meV multiplied by the empirical factor of ≈ 0.8–0.9.[17] This leads to the ratio $2\Delta/k_BT_c=3.1$–3.5, which is consistent with that for the higher-T_c phase in RNi_2B_2C.

From the measurements of the temperature dependence of the tunneling conductance as shown in Figs. 7, 9, 13, and 14, it is obvious that the distribution of the gap value is due to the T_c difference probably arising from local variations of stoichiometry. Such features have also been found in the cuprate single crystals, which have been preventing us from obtaining the intrinsic properties of the tunneling spectra.[17]

We have occasionally observed the large gap feature of $eV_{\mathrm{p.-p.}}=18$ meV at 4.2 K in YNi_2B_2C as shown in Fig. 16. The background conductance is asymmetric and strongly bias dependent, but the subgap conductance is well decreased with the substantial overshoots at the gap edges that are much broadened. The value of $R_J\approx 50\ \mathrm{k}\Omega$ at ± 20 mV is

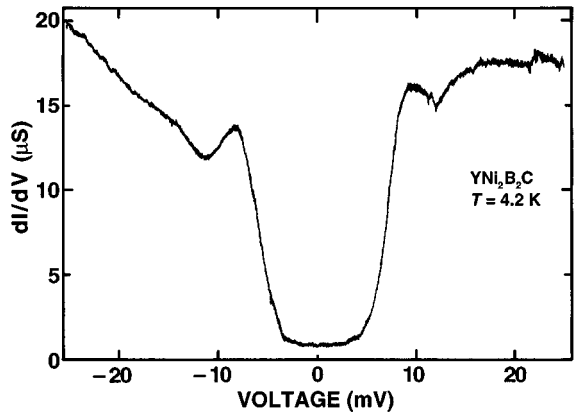

FIG. 16. Tunneling conductance for an YNi_2B_2C break junction showing the largest-gap feature in the present work.

similar to that of the other data in the present work, and the positions of the gap structures were reproducible for the different junctions with R_J (± 20 mV) up to ≈ 400 kΩ. Therefore this is considered to be due to the superconducting gap, and the possibility of observing the nonintrinsic effect such as a Coulomb blockade can be excluded, although the conservation of the areas below and above the gap energies seems to be difficult to confirm because of the strongly bias-dependent background-conductance feature. Since $eV_{\text{p.-p.}}=18$ meV is twice as large as $4\Delta_{\text{p.-p.}}/e$ of Fig. 1, it can be primarily due to double SIS tunneling. Within this interpretation, the ratio $2\Delta_{\text{p.-p.}}/k_BT_c \approx 3.5$ is obtained with a bulk T_c of about 15 K. We note that the existence of the higher-T_c phase as was found in YPd_2B_2C (Ref. 4) also cannot be ruled out as the origin of the large gap value, because tunneling spectroscopy could probe local quasiparticle excitations very sensitively. This is supported by the observation of the low-T_c gaps as is already presented in this work.

In contrast to the present results of the BCS gap size in $R\text{Ni}_2\text{B}_2\text{C}$, deviations from BCS behavior have been discussed in some reports.[7,9,20] From the normalized specific-heat discontinuity of $\Delta C/\gamma T_c=1.6-1.8$ reported by Carter *et al.*,[7] which is larger than the BCS value of 1.43, the ratio $2\Delta/k_BT_c=3.7-3.9$ is obtained using $\Delta C/\gamma T_c \approx 0.115(2\Delta/k_BT_c)^2$.[33] This result points to an intermediate-to-strongly coupled superconductivity. Furthermore, the temperature dependence of the electronic contribution to the specific heat (C_e) in the superconducting states for $R\text{Ni}_2\text{B}_2\text{C}$ by Hong *et al.* seems to obey a power law with $C_e/\gamma T_c \approx t^{2.75}$, rather than the BCS activation formula $C_e/\gamma T_c \approx 8.5\exp[-0.82\Delta(0)/k_BT]$ at low temperatures of $t<0.3$.[7] The temperature dependence of the nuclear spin-lattice relaxation rate $1/T_1$ of ^{11}B showed no enhancement just below T_c with the magnetic field down to 0.4 T, and its temperature dependence seems to be consistent with a power law rather than the BCS activation type.[20] These results are not consistent with the present tunneling measurements. However, we believe that the above results are due to local variations of stoichiometry or normal-state impurities which would cause low-energy quasiparticle excitations as a result of pair breaking.

There exists a calculation that predicts the existence of high-energy phonons to give the estimation of a large electron-phonon coupling constant λ (up to 2.6).[9] The large λ value implies low-energy phonons which would be caused by a softening of the B phonon mode or the phonons from heavy ions.[9] Such a strong electron-phonon interaction ($\lambda > 1-1.5$) would result in the ratio $2\Delta/k_BT_c \approx 4-4.6$, where the structures of the electron-phonon interaction must be observable above the gap energies in the tunneling conductance with about 2–3 % deviations from the BCS density of states, as is seen for Pb and $A15$ compounds.[6,15] However, the above prediction of a large λ is also not consistent with our tunneling results of a weak-coupling superconductivity, as well as no phonon structures in the tunneling data. It is, therefore, of practical interest to compare $R\text{Ni}_2\text{B}_2\text{C}$ with other strong-coupling intermetallic $A15$ compounds like Nb_3Sn using the same experimental technique. Preliminary results of our break-junction measurements have given the results of $2\Delta=6.7$ meV at 4.2 K with $T_c=17.3$ K of the junction, thereby giving a strong-coupling value of $2\Delta/k_BT_c=4.5$.[34] This value agrees well with the literature[6] and clearly distinguishes Nb_3Sn from $R\text{Ni}_2\text{B}_2\text{C}$ in spite of having the similar $T_c=15-17$ K. It is noted that the Chevrel-phase compounds with $T_c=10-12$ K have been also reported to be very strong-coupling superconductors with $2\Delta/k_BT_c=4-5$,[16] but by taking into account the broadening feature of the tunneling spectra,[17] the ratio is turned out to fall into a weak-to-moderate coupling regime of 3.5–3.8. This is rather in agreement with that of $R\text{Ni}_2\text{B}_2\text{C}$ than Nb_3Sn. Note here that the γ value of $R\text{Ni}_2\text{B}_2\text{C}$ is similar to that of the $A15$ compounds, but is smaller than that of the Chevrel compounds.[8]

We here briefly mention the present results of $2\Delta/k_BT_c=3.5$ obtained for $R\text{Ni}_2\text{B}_2\text{C}$. The BCS gap value for a wide T_c range of 5–16 K for $R\text{Ni}_2\text{B}_2\text{C}$ is similar to that for $Ba_{1-x}K_xBiO_3$ throughout $T_c=15-30$ K.[29] This is in contrast to the case of the intermetallic $A15$ compounds Nb_3Ge where $2\Delta/k_BT_c$ increases rapidly from the value slightly below 3.5 ($T_c=7-12.6$ K) to a strong-coupling value of 4.3–4.5 at the stoichiometric phase boundary ($T_c=21.2$ K).[6] From the semiempirical formula of the strong-coupling correction for $2\Delta/k_BT_c$ given by Mitrovic *et al.*[35] using the Eliashberg equations

$$2\Delta/k_BT_c=3.5[1+12.5(k_BT_c/E_{\ln})^2\ln(E_{\ln}/2k_BT_c)] \quad \text{for } k_BT_c/E_{\ln}<0.3), \tag{5}$$

with

$$E_{\ln}=\exp\left[(2/\lambda)\int F(E)(\ln E/E)dE\right]$$

[$F(E)$ is the phonon density of states], its variation with respect to T_c for the same material in the strong-coupling region can be arised from whether T_c is a function of $E_{\ln}$ or not. For Ni_2B_2C, the measurements of the isotope effect YNi_2B_2C showed a large shift of T_c for B atoms. This suggests the dominant role of high-energy phonons such as boron a_{1g} optical mode[14] involving the dynamical modulation of the NiB_4 tetrahedral bond angles as is predicted by the band-structure calculation.[10] Therefore the condition $k_BT_c \ll E_{\ln}$ seems to be realized because of the possible contributions of the high-energy phonons arising from the light mass B as well as C atoms. The more detailed tunneling measurements combined with the inelastic-neutron- and Raman-scattering measurements of the phonon spectra will be helpful to confirm this conjecture.

SUMMARY

We have investigated the superconducting energy gap in $R\text{Ni}_2\text{B}_2\text{C}$ using the break-junction tunneling technique. The observed low-temperature characteristics as well as the temperature dependence of the gap are well described by the BCS theory. In particular, the tunneling conductance is almost fully explained by the lifetime-broadened BCS density of states without any additional leakage conductance, thereby giving evidence for an unaffected junction interface other than the grain boundary effect. The several gap values observed at low temperatures are found to be due to the T_c distributions. This is because stoichiometry variations in a small area tend to occur for these multicomponent polycrystalline compounds, which cannot be probed by both the x-ray

and SQUID measurements. With the aid of this characteristic, the T_c dependence of the gap is obtained. The ratio $2\Delta/k_BT_c=3.5$ is found to be kept constant with changes in T_c from 4.6–15 K, indicating a weak-coupling, BCS, superconductivity for $R\mathrm{Ni}_2\mathrm{B}_2\mathrm{C}$. We were not able to obtain clear evidence for the electron-phonon interaction in the tunneling spectra, even if we succeeded in obtaining the very-sharp-gap structures. Measurements using single crystals will be needed to explore this issue further.

ACKNOWLEDGMENTS

This work was supported by a Grant-in-Aid for Scientific Research from the Ministry of Education, Science and Culture, Japan. Aoyama-Gakuin University is partly supported by the New Energy and Technology Development Organization (NEDO). One of the authors (M.K.) was partially supported by the Japan Society for the Promotion of Science for Young Scientists.

*Electronic address: ekino@ue.ipc.hiroshima-u.ac.jp

[1] R. Nagarajan, C. Mazumdar, Z. Hossain, S. K. Dhar, K. V. Gopalakrishnan, L. C. Gupta, C. Godart, B. D. Padalia, and R. Vijayaraghavan, Phys. Rev. Lett. **72**, 274 (1994).

[2] R. J. Cava, H. Takagi, H. W. Zandbergen, J. J. Krajewski, W. F. Peck, Jr., T. Siegrist, B. Batlogg, R. B. van Dover, R. J. Felder, K. Mizuhashi, J. O. Lee, H. Eisaki, and S. Uchida, Nature **367**, 252 (1994).

[3] T. Siegrist, H. W. Zandbergen, R. J. Cava, J. J. Krajewski, and W. F. Peck, Jr., Nature **367**, 254 (1994).

[4] R. J. Cava, H. Takagi, B. Batlogg, H. W. Zandbergen, J. J. Krajewski, W. F. Peck, Jr., R. B. van Dover, R. J. Felder, T. Siegrist, K. Mizuhashi, J. O. Lee, H. Eisaki, S. A. Carter, and S. Uchida, Nature **367**, 146 (1994).

[5] H. W. Zandbergen, T. J. Gortenmulder, J. L. Sarrac, J. C. Harrison, M. C. de Andrade, J. Hermann, S. H. Han, Z. Fisk, M. B. Maple, and R. J. Cava, Physica C **232**, 328 (1994).

[6] J. Kwo and T. H. Geballe, Phys. Rev. B **23**, 3230 (1981); Physica **109&110B**, 1665 (1982).

[7] S. A. Carter, B. Batlogg, R. J. Cava, J. J. Krajewski, and W. F. Peck, Jr., Phys. Rev. B **50**, 4216 (1994); N. M. Hong, H. Michor, M. Vybornov, T. Holubar, P. Hundegger, W. Perthold, G. Hilscher, and P. Rogl, Physica C **227**, 85 (1994).

[8] H. Takagi, R. J. Cava, H. Eisaki, J. O. Lee, K. Mizuhashi, B. Batlogg, S. Uchida, J. J. Krajewski, and W. F. Peck, Jr., Physica C **228**, 289 (1994).

[9] W. E. Pickett and D. J. Singh, Phys. Rev. B **72**, 3702 (1994).

[10] L. F. Mattheiss, T. Siegrist, and R. J. Cava, Solid State Commun. **91**, 587 (1994).

[11] T. Hasegawa, M. Ogino, A. Takagi, E. Watanabe, M. Naitoh, H. Takagi, S. Uchida, R. J. Cava, and K. Kitazawa, Physica C **235–240**, 1859 (1994).

[12] T. Ekino, H. Fujii, M. Kosugi, Y. Zenitani, and J. Akimitsu, Physica C **235–240**, 2529 (1994).

[13] L. F. Rybaltchenko, I. K. Yanson, A. G. M. Jansen, P. Mandal, P. Wyder, and C. V. Tomy, Physica B (to be published).

[14] D. D. Lawrie and J. P. Franck, Physica C **245**, 159 (1995).

[15] E. L. Wolf, *Principles of Electron Tunneling Spectroscopy* (Oxford University Press, New York, 1985).

[16] U. Poppe and H. Wuhl, J. Low Temp. Phys. **43**, 371 (1981).

[17] T. Ekino and J. Akimitsu, in *Studies of High Temperature Superconductors*, edited by A. V. Narlikar (Nova Science, New York, 1992), Vol. 9, p. 259; *Superconductivity*, in *Frontiers of Solid State Sciences* Vol. 1, edited by L. C. Gupta and M. S. Multani (World Scientific, Singapore, 1993), p. 477.

[18] N. Grewe and F. Steglich, in *Handbook on the Physics and Chemistry of Rare Earths*, edited by K. A. Gschneidner, Jr. and L. Eyring (Elsevier, New York, 1991), Vol. 14, p. 343.

[19] T. Ekino, T. Takabatake, H. Tanaka, and H. Fujii, Phys. Rev. Lett. **75**, 4262 (1995).

[20] M. E. Hanson, F. Lefloch, W. H. Wong, and W. G. Clark, Phys. Rev. B **51**, 674 (1995); T. Kohara, T. Oda, K. Ueda, Y. Yamada, A. Mahajan, K. Elankumaran, Z. Hossian, L. C. Gupta, R. Nagarajan, R. Vijayaraghavan, and C. Mazumdar, *ibid.* **51**, 3985 (1995).

[21] A. A. Menovsky, C. E. Snel, T. J. Gortenmulder, H. J. Tan, and T. T. M. Palstra, J. Cryst. Growth **74**, 231 (1986).

[22] M. Ishikawa, H. Takahashi, T. Satho, and M. Takigawa, J. Magn. Magn. Mater. **63&64**, 351 (1987).

[23] R. C. Dynes, V. Narayanamurti, and J. P. Garno, Phys. Rev. Lett. **41**, 1509 (1978).

[24] S. Arisawa, T. Hatano, K. Hirata, T. Motiku, H. Kitaguchi, H. Fujii, H. Kumakura, K. Kadowaki, K. Nakamura, and K. Togano, Appl. Phys. Lett. **65**, 1299 (1994).

[25] S. M. Freake, Philos. Mag. **24**, 319 (1971).

[26] N. van der Post, E. T. Peters, I. K. Yanson, and J. M. van Ruitenbeek, Phys. Rev. Lett. **73**, 2611 (1994).

[27] N. Agrait, J. G. Rodrigo, and S. Vieira, Phys. Rev. B **46**, 5814 (1992).

[28] G. E. Blonder, M. Tinkham, and T. M. Klapwijk, Phys. Rev. B **25**, 4515 (1982).

[29] M. Kosugi, J. Akimitsu, T. Uchida, M. Furuya, Y. Nagata, and T. Ekino, Physica C **229**, 389 (1994).

[30] M. Xu, P. C. Canfield, J. E. Ostenson, D. K. Finnemore, B. K. Cho, Z. R. Wang, and D. C. Johnston, Physica C **227**, 321 (1994).

[31] T. Takabatake, Y. Maeda, T. Konishi, and H. Fujii, J. Phys. Soc. Jpn. **63**, 2853 (1994).

[32] S. L. Bud'ko, M. Elmassalami, M. B. Fontes, J. Mondragon, W. Vanoni, B. Giordanengo, and E. M. Baggio-Saitovitch, Physica C **243**, 183 (1995).

[33] M. Tinkham, *Introduction to Superconductivity* (McGraw-Hill, New York, 1975).

[34] T. Ekino *et al.* (unpublished).

[35] B. Mitrovic, H. G. Zarate, and J. P. Carbotte, Phys. Rev. B **29**, 184 (1984).